



Contents lists available at *Dergipark*

Journal of Scientific Reports-A

journal homepage: <https://dergipark.org.tr/tr/pub/jsr-a>



E-ISSN: 2687-6167

Number 61, June 2025

RESEARCH ARTICLE

Receive Date: 16.01.2025

Accepted Date: 29.05.2025

Analysis of LiDAR system performance through analogy with FSO communication systems

Bünyamin Kaya^{a*}, Ahmet Altuncu^b

*^aKütahya Dumlupınar University, Department of Electric- Electronic Engineering, Kütahya
Nursan Kablo Donanımları San. ve Tic. A.Ş. Kütahya 43300, Türkiye
ORCID: 0000-0002-9907-2826*

*^bAfyon Kocatepe University, Department of Electric-Electronic engineering, Afyonkarahisar, Türkiye
ORCID: 0000-0002-3753-9515*

Abstract

LiDAR (Light Detection and Ranging) systems are used in autonomous vehicle technology and environmental sensing applications. In this study, the performance of LiDAR systems is simulated by adapting it to a free space optical (FSO) communication system and analyzed using this approach. OptiSystem software was used in the simulation studies and different atmospheric conditions such as clear, rainy and extremely foggy weather conditions were considered. The performance of LiDAR systems under these conditions was evaluated; the effects of features on the backscattering ratios of the backscattered signals from the target surface and the effects of these outputs on system performance were evaluated. The results were analyzed to show that atmospheric conditions and target reflection rates affect the LiDAR system performance and that the received pulse quality is negatively affected by increasing the detection distance.

© 2023 DPU All rights reserved.

Keywords: LiDAR; Free-Space Optical Communication; FSO; BER Analysis; OptiSystem Simulation; Performance Analysis.

1. Introduction

Optical communication systems have attracted significant attention due to their ability to provide high-speed data transmission with low latency and high reliability. In addition to conventional fiber-optic systems, Free Space Optical

* Corresponding author. Tel.: +0 555-641-23-77;
E-mail address: bunyasacademy@gmail.com

(FSO) systems have emerged as a flexible, energy-efficient [1] and high-bandwidth alternatives that operate without the need for fiber waveguides, relying instead on FSO-based propagation principles [2,3,4].

However, the performance of FSO systems is significantly affected by absorption, scattering and turbulence-induced degradation [5,6,7,8], and the stability and reliability of FSO links are also adversely impacted by environmental factors such as rain, fog, snow, dust and high particulate concentrations in the atmosphere [9,10].

Specifically, in low density foggy and dusty environments, the system can provide successful transmission over longer distances, while the transmission distance is significantly shortened in medium and high density foggy and dusty conditions [11,12]. Consequently, the Bit Error Rate (BER) increases while the Q-Factor decreases.

Similarly, LiDAR (Light Detection and Ranging) is a technology that uses laser beams to perform high-resolution and precise distance measurements and can operate under various atmospheric conditions. Therefore, LiDAR systems are widely used in applications such as environmental sensing and object recognition in next-generation autonomous vehicles [13].

Due to the propagation of laser beams through the atmosphere and their reliance on reflections from objects, LiDAR systems, like FSO systems, are affected by atmospheric conditions. This leads to performance degradation in terms of detection range and accuracy [8,14,15,16].

For instance, in [17], sensitivity and accuracy evaluations were carried out using different reflective targets in the range of 5 to 180 m, and it was shown that in many systems, the detection capability decreases with increasing distance depending on the reflectivity.

Similarly, [13] also emphasises the effect of atmospheric conditions on detection accuracy and the importance of signal processing methods. In [18], Optical Code Division Multiple Access (OCDMA) technology was proposed to mitigate mutual interference effects in LiDAR systems, reducing the false alarm rate from 90% to 2%. Additionally, using a Lambert surface model and a theoretical analysis method, the effects of parameters such as interference distance and angle on detection and false alarm performance were examined in detail [19].

The optical similarities between LiDAR and FSO systems—including shared components and atmospheric behavior—are key to enabling accurate cross-domain modeling and performance prediction. Therefore, the analogy between LiDAR system parameters and FSO communication systems offers opportunities for both the performance evaluation of existing systems and the development of next-generation technologies.

In this study, unlike the communication-oriented FSO analyses in the literature, the FSO channel structure is analysed by analogy to evaluate the LiDAR detection performance. The analogy relates FSO and LiDAR systems from both a performance-based evaluation perspective and a sensing performance enhancement perspective. In this context, the performance parameters of LiDAR systems are compared with those of FSO communication systems, and analyses were conducted using the OptiSystem V21 software. In this simulation, a lens-free LiDAR system is implemented by inserting a coreless fiber tip spliced at the end of optical transmission fiber cable with 0.125 mm cladding diameter to serve as optical transmitter and receiver pairs with a constant aperture diameter in the given FSO channel. Although there are several experimental studies showing the channel behavior of FSO systems under different atmospheric conditions, studies conducted by drawing an analogy to LiDAR systems are very limited. The aim of this study is both to develop a simulation model that resembles a LiDAR system using the FSO model and to use this model for a lens-free, fully optical fiber based LiDAR design capable of short-range detection, by employing coreless fiber tips spliced to fiber cables as transmitter and receiver apertures. In the simulations conducted using the proposed LiDAR design, various atmospheric conditions (clear, rainy, and foggy weather conditions) and target reflectivity levels (10%, 35%, 60%, 90%) were considered, and the results have shown the critical factors affecting the performance of LiDAR systems.

2. Method

The LiDAR-FSO system model used in the simulations is given schematically in Figure 1. The LiDAR-FSO system model created in OptiSystem V21 software is also shown in Figure 2. Detailed information about the subsystem parameters used in OptiSystem V21 software is given in Table 1.

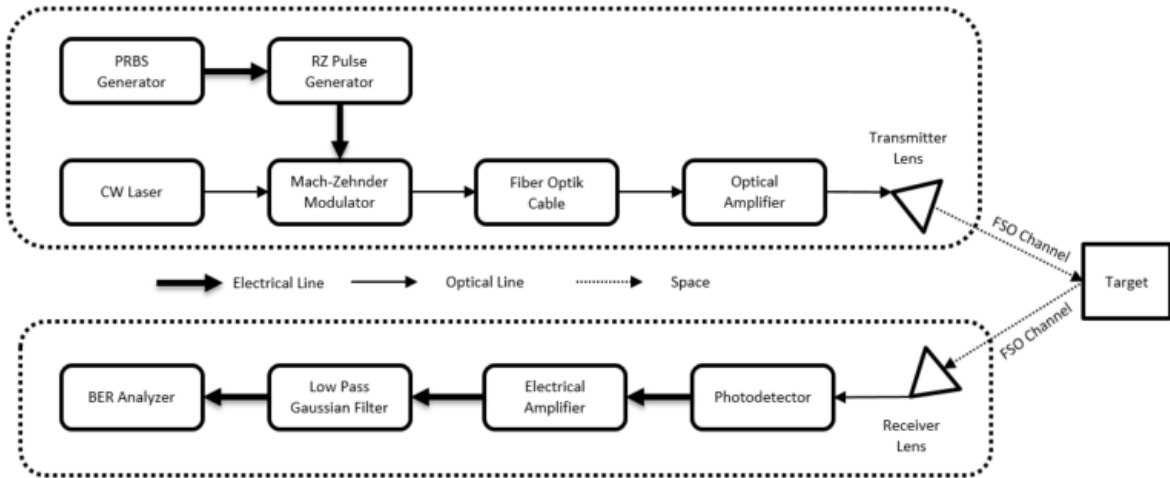


Fig. 1. LiDAR-FSO system model

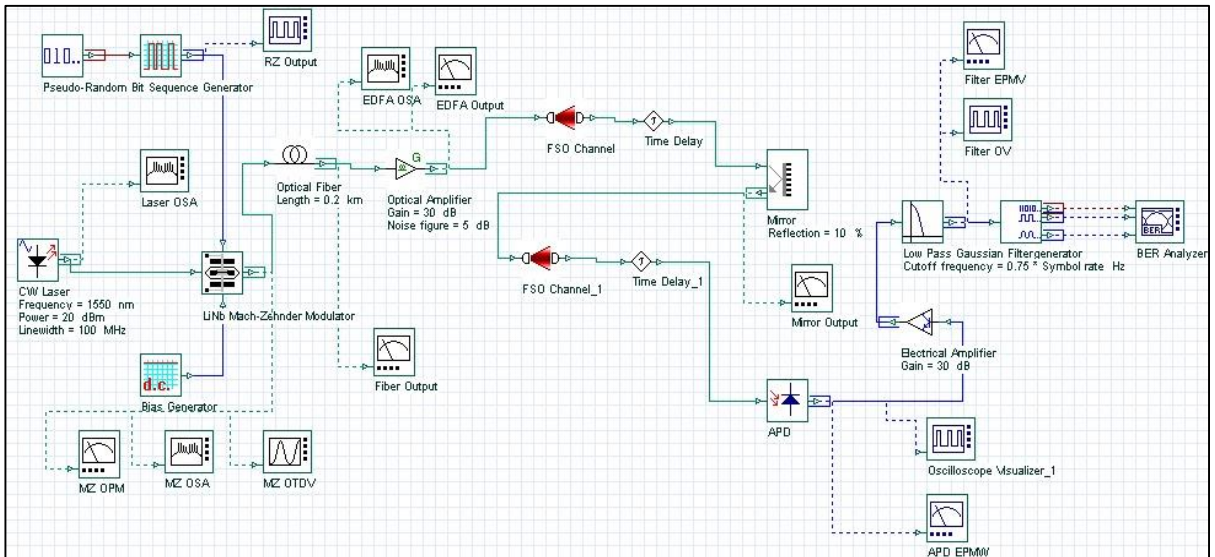


Fig. 2. LiDAR-FSO simulation schematics realized in OptiSystem V21.

Table 1. Subsystem specifications used in the simulations.

Product Name	Parameters	Its function in the LiDAR-FSO System
Pseudo-random bit sequence generator.	Bit rate: 1+E6 bit/s.	Provides PRBS data for modulation of the transmitted signal in the LiDAR-FSO system.
RZ-pulse generator.	Duty cycle: 0.01 bit.	It functions as a pulse shaper to generate RZ-type LiDAR pulses.
CW laser.	Wavelength : 1550 nm, output power: +20 dBm, linewidth: 100 MHz.	A CW laser source with a low loss and eye-safe wavelength in the atmosphere for LiDAR-FSO applications (1550 nm).
Mach-Zehnder modulator.	LiNbO3 MZ modulator with a variable bias input.	It allows generation of LiDAR pulses in the form of RZ-modulated PRBS data.
Optical amplifier (EDFA).	Gain: 30 dB, noise figure: 5 dB.	Enhances the optical LiDAR pulse power to compensate for the losses in the LiDAR-FSO channel.
Optical fiber.	Length: 0.2 km, standard single-mode fiber (S-SMF) link with attenuation of 0.2 dB/km and dispersion of 16.75 ps/nm/km.	It is used to transmit LiDAR pulses to the FSO transmitter.
FSO channel.	Distance: 20-30-40-50-60-70-80 m, attenuation: 1.875 - 12.5 - 18.75 dB/km. Transmitter and receiver aperture diameter: 0.125 mm (coreless fiber diameter).	It models the FSO link at optical frequencies under different atmospheric conditions resembling LiDAR systems.
Mirror reflector.	Reflection: 10% - 35% - 60% - 90% [20].	It simulates the back reflections arising from the other vehicles and obstacles in the LiDAR system.
APD (Avalanche photodiode).	High sensitivity and responsivity at 1550 nm.	It converts low pulse energy LiDAR pulses reflected back into electrical pulses.
Electrical amplifier.	30 dB gain.	Enhances the electrical LiDAR pulses.
Low pass filter.	Cut frequency: 0.75 x symbol rate.	Improves SNR in LiDAR signals by reducing out-of-band noise.
BER analyzer.	Bit error rate measurement.	It analyses the BER performance of the FSO channel resembling to LiDAR system.

2.1. FSO channel model

FSO Channel is a subsystem consisting of an FSO transmitter with a variable aperture, a free space link with variable atmospheric parameters, and an FSO receiver with a variable aperture. In the designed system, two FSO links were used resembling the links from the transmitter to the mirror reflector and from the mirror reflector to the receiver [3]. The FSO link parameters include the propagation distance between 20-80 m for one way, free space attenuation under different atmospheric conditions such as clear, rainy, and foggy weather, and transmitter and receiver aperture diameters. In the FSO channel, the transmitter and receiver aperture diameters were kept at 0.125 mm resembling a coreless fiber tip emitter/collector under the scenario of a fiber-coupled LiDAR system.

FSO channel has two main effects on the transmission of LiDAR pulses. The first parameter is power attenuation of the laser light in the atmosphere under different weather conditions. The second parameter is geometric loss and occurs due to the divergence of the transmitted beam between the transmitter and receiver. It is calculated using the aperture diameters of the transmitter and receiver and the beam divergence angle, as shown in Equation 1[3], and [21].

$$P_{Received} = P_{Transmitted} \cdot \frac{d_R^2}{[d_T + (D-R)]^2} \cdot 10^{\left(\frac{-\alpha\beta}{10}\right)} \cdot 10^{\left(\frac{-TX}{10}\right)} \cdot 10^{\left(\frac{-RX}{10}\right)} \cdot 10^{\left(\frac{-AD}{10}\right)} \quad (1)$$

Where:

- $P_{Received}$: Received Power (W)
- $P_{Transmitted}$: Transmitted Power (W)
- d_T : Transmitter aperture diameter (m)
- d_R : Receiver aperture diameter (m)
- D : Beam divergence (mrad)
- R : Range (km)
- α : Atmospheric attenuation (dB/km)
- TX : Transmitter Loss (dB)
- RX : Receiver Loss (dB)
- AD : Additional Losses (dB)

In the simulations, the losses at the fiber-lens interface in the transmitter and lens-fiber interface in the receiver, i.e. coupling losses, are defined as transmitter loss (TX) and receiver loss (RX). Additional losses arising from scintillation, misalignment and other factors, is specified as Additional Losses (AD).

The propagation delay parameter enables to account the atmospheric turbulence effects between the transmitter and the receiver and therefore is included in the LiDAR-FSO model. To model atmospheric fading, which depends on intensity scintillation, a Gamma-Gamma distribution was used [21]. The probability of a given Intensity I is defined in Equation 2 [22].

$$P(I) = \frac{2(\alpha\beta)^{\frac{(\alpha+\beta)}{2}}}{\Gamma(\alpha) \cdot \Gamma(\beta)} \cdot I^{\frac{\alpha+\beta}{2}-1} \cdot K_{(\alpha-\beta)}(2\sqrt{(\alpha\beta)I}) \quad (2)$$

where, $1/\alpha$ and $1/\beta$ represent the variances of small-scale and large-scale turbulence, respectively [21] as defined in Equations 3 and 4. [23] $\Gamma(x)$ denotes the Gamma function, and $K_{\alpha-\beta}(x)$ represents the modified Bessel function of the second kind.

$$\alpha = \exp \left[\frac{0,49\sigma R^2}{\left(1+0,69\sigma R^{\frac{12}{5}}\right)^{\frac{7}{6}}} \right] - 1 \quad (3)$$

$$\beta = \exp \left[\frac{0,51\sigma R^2}{\left(1+0,69\sigma R^{\frac{12}{5}}\right)^{\frac{7}{6}}} \right] - 1 \quad (4)$$

The Rytov variance is calculated from:

$$\sigma R^2 = 1,23 C_n^2 k^{\frac{7}{6}} z^{\frac{11}{6}} \quad (5)$$

Here, the value of C_n^2 is the refractive index structure parameter, which ranges from $10^{-13} \text{ m}^{-2/3}$ for strong turbulence to $10^{-17} \text{ m}^{-2/3}$ for weak turbulence, k represents the optical wave number, and z is the parameter Range. Channel time variations are considered based on the theoretical quasi-static model, also known as the frozen channel model. According to this model, channel fading is assumed to remain constant over one symbol frame (coherence time) and changes to a new independent value from one frame to the next. [23]

2.2. Simulation results

In this study, firstly, the scenarios with different reflection ratios from the target surface (%10, %35, %60, and %90) were examined and the effect of reflection ratio on system performance was analyzed. During the simulations, the following parameters were used: a bit rate of 10 kbps, a duty cycle of 0.01, and a pulse width of 10 ns. The atmospheric attenuations based on weather conditions were determined as follows: 1.875 dB/km for clear weather, 12.5 dB/km for rainy weather, and 18.75 dB/km for dense foggy weather. The Q factor and BER variations obtained for different reflection ratios are given in Fig.3 as a function of mirror (target) distance. As shown in Fig.3, at a 10% reflection ratio, a reflecting pulse signal with a very low intensity was received from the target surface and hence this has caused a significant decrease in Q factor and an increase in BER value. It was observed that Q-Factor decreases to the accepted minimum value of 6 when the one-way distance (range) of the target was 60 m for clear weather, 55 m for rainy weather and 50 m for extremely foggy weather. The low reflection ratio of the target surface made the signal detection process more challenging as the distance increased, which, in turn, caused a considerable rise in bit error rates.

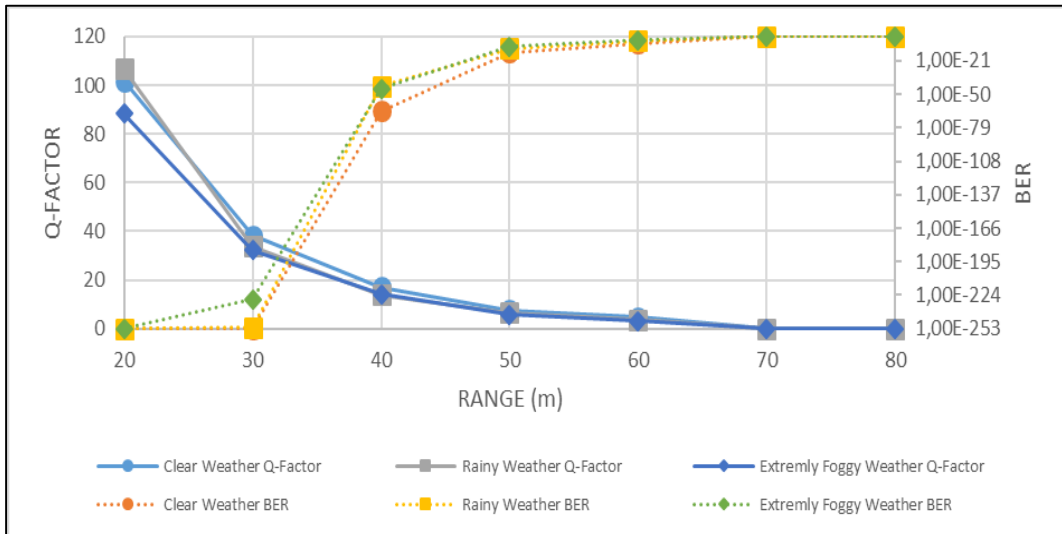


Fig. 3. Q-Factor and BER variation as a function of mirror (target) distance obtained under three atmospheric weather conditions (clear, rainy and extremely foggy weather) for the mirror reflection ratio of 10%.

Increasing the reflection ratio to 35% resulted in a significant improvement in system performance. As shown in Fig. 4, when the target's one-way distance (range) was 75m in clear weather, 65m in rainy weather, and 60m in extremely foggy weather, the Q-Factor was observed to drop to the minimum acceptable value of 6. This improvement was supported by an overall increase in Q-Factor and a decrease in BER value.

However, signal attenuation in rainy and extremely foggy weather conditions is higher. While the adverse effects on transmission performance were less pronounced compared to a 10% reflection rate, they still poses significant challenges to the system. Specifically, compared to the 10% reflection rate, difficulty in pulse detection has been reduced, and therefore BER performance improved. Nonetheless, it was evident that performance losses caused by environmental factors could not be eliminated.

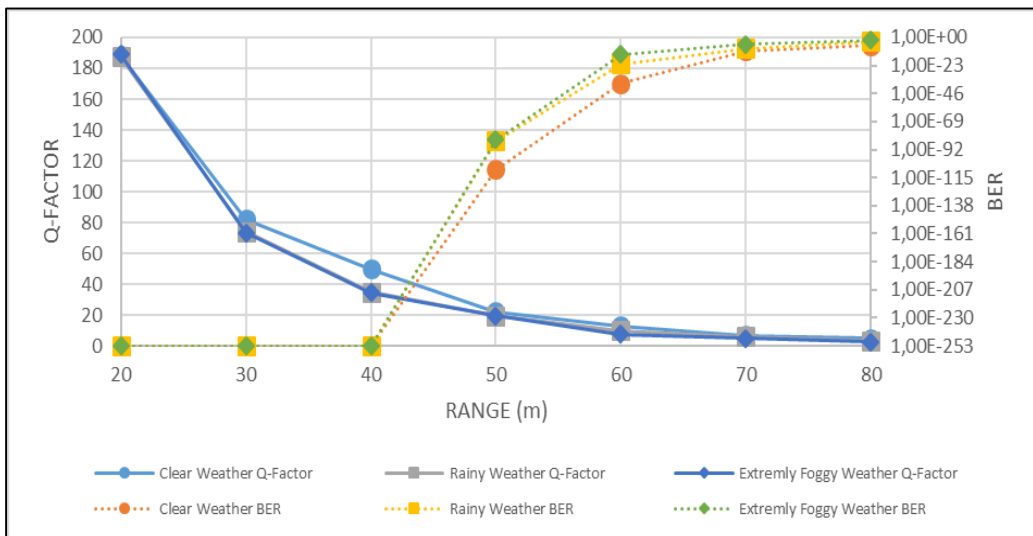


Fig. 4. Q-Factor and BER variation as a function of the mirror (target) distance obtained under three atmospheric weather conditions (clear, rainy and extremely foggy weather) for the mirror reflection ratio of 35%.

Increasing the mirror reflection ratio to 60% resulted in a significant improvement in signal transmission performance. As shown in Fig. 5, when the target's one-way distance (range) was 85m in clear weather, 80m in rainy conditions, and 75m in extremely foggy weather, the Q-Factor was observed to drop to the minimum acceptable value of 6.

Under clear weather conditions, Q-Factor values reached remarkably high levels, and the BER dropped to a minimum. In rainy weather, while transmission performance was more affected, Q-Factors and BER values have remained at acceptable levels. However, in extremely foggy weather condition, transmission performance continued to be adversely affected, leading to a significant decrease in Q factor and a noticeable increase in BER.

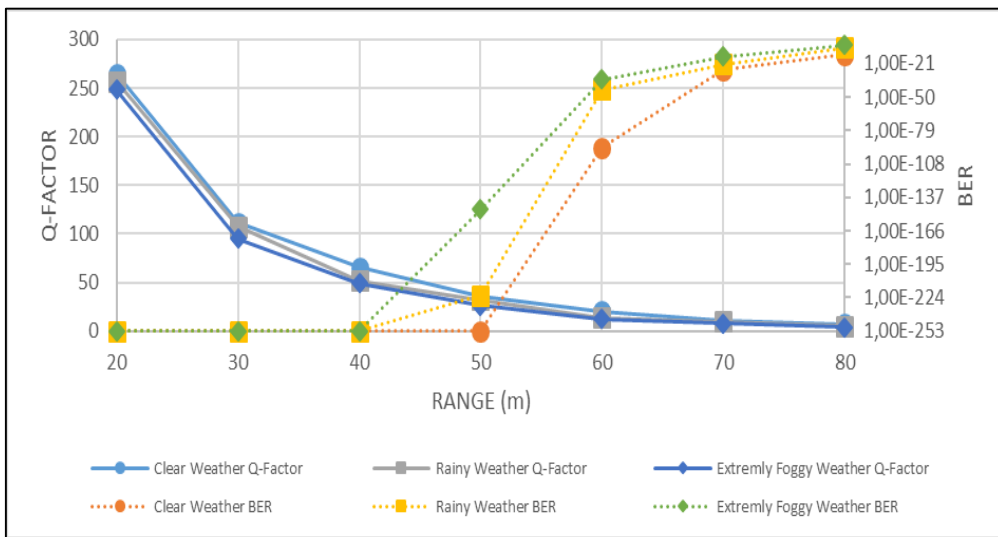


Fig. 5. Q-Factor and BER variation as a function of mirror (target) distance obtained under three atmospheric weather conditions (clear, rainy and extremely foggy weather) for the mirror reflection ratio of 60%.

Increasing the reflection ratio to 90% enabled perfectly receiving the strongly reflected pulses from the target surface, bringing transmission performance to its maximum level. As shown in Fig. 6, when the target's one-way distance (range) was 95m in clear weather, 85m in rainy conditions, and 80m in extremely foggy, the Q-Factor was observed to drop to the minimum acceptable value of 6.

Under clear weather conditions, Q-Factor values reached to maximum levels, and corresponding BER values have reduced to nearly zero. In rainy weather conditions, while system performance was slightly affected, it continued to operate with high Q factors. Even under extremely foggy conditions, the 90% reflection ratio has demonstrated an acceptable performance compared to less reflection ratios, with significantly improved signal detection and less BERs.

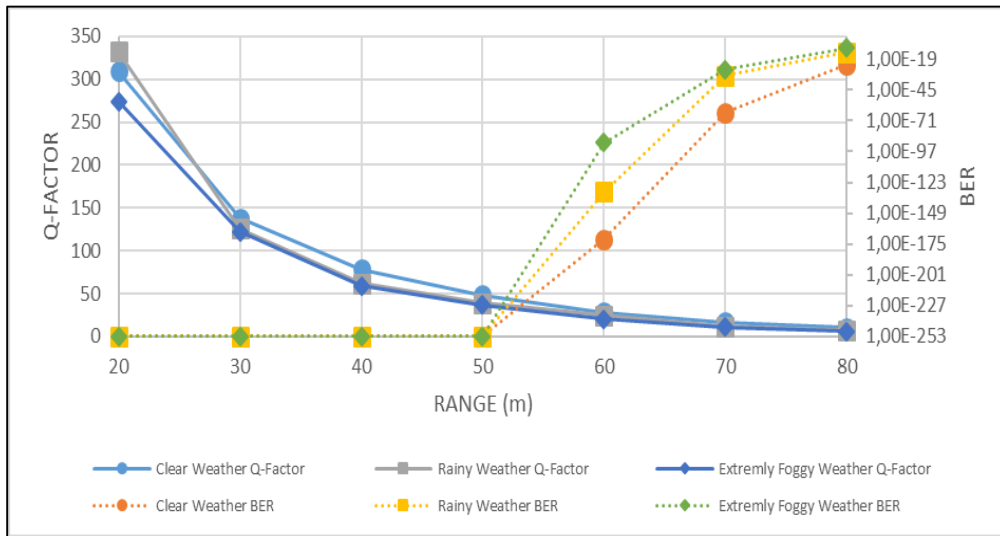


Fig. 6. Q-Factor and BER variation as a function of mirror (target) distance obtained under three atmospheric weather conditions (clear, rainy and extremely foggy weather) for the mirror reflection ratio of 90%.

In this study, secondly, the eye diagrams of the received pulses were obtained which play a critical role in evaluating signal quality under different LiDAR-FSO link conditions [15]. The received signal eye diagram was obtained under clear, rainy, and extremely foggy weather conditions together with the corresponding Q-Factors. Figures 7. a, b, c, and d display the eye diagrams of the received pulses under clear weather condition when the mirror reflection ratios are 10%, 35%, 60%, and 90%, respectively, for a target distance of 50 m. Measured Q factor and BER value are also given for each specific condition. The eye diagrams obtained show that an increase in the reflection ratio of the mirror leads to a significant improvement in back-reflected pulse quality, highlighting this parameter as a key factor influencing the performance of LiDAR-FSO systems. Although the level of obtained Q factors are sufficient for a reliable sensing of LiDAR back-reflected pulse, the intensity of the noise is significantly high for the reflection ratio of 10%.

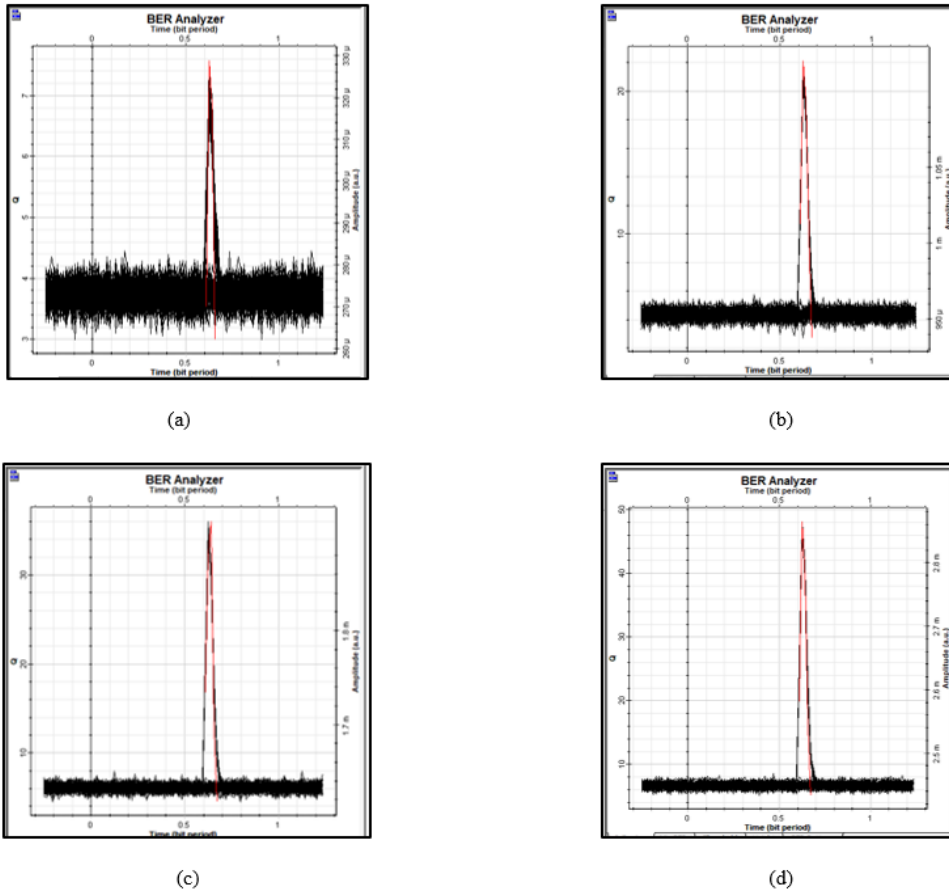


Fig. 7. (a). Eye diagram of the received signal obtained under clear weather condition for 10% reflection from the target, measured Q-Factor = 7.57, BER = 1.78e-14. (b). Eye diagram of the received signal obtained under clear weather condition for 35% reflection from the target, measured Q-Factor = 22.12, BER = 8.53e-109. (c). Eye diagram of the received signal obtained under clear weather condition for 60% reflection from the target, measured Q-Factor = 36.03, BER = 1e-253. (d). Eye diagram of the received signal obtained under clear weather condition for 90% reflection from the target, measured Q-Factor = 48.15, BER = 1e-253.

Under rainy weather conditions, Figures 8. a, b, c, and d illustrate the eye diagrams of pulses received at a 50 m target distance, with mirror reflection ratios of 10%, 35%, 60%, and 90%, respectively. The obtained eye diagrams clearly demonstrate that increasing the reflection ratio significantly improves back-reflected and received signal quality in rainy weather conditions, highlighting the critical role of this parameter in the performance of LiDAR-FSO systems.

While the Q-Factor achieved at each reflection ratio is sufficiently high for a reliable detection of the LiDAR back-reflected pulses, the noise intensity in rainy weather conditions is noticeably higher for all reflection ratios compared to clear weather. Specifically, at a 10% reflection rate, the noise level is significantly high, making the signal detection more challenging than under clear weather condition. These findings show that increasing the reflection ratio is not only crucial for optimizing LiDAR-FSO system performance in clear weather but also is required for improving received signal quality in rainy weather conditions.

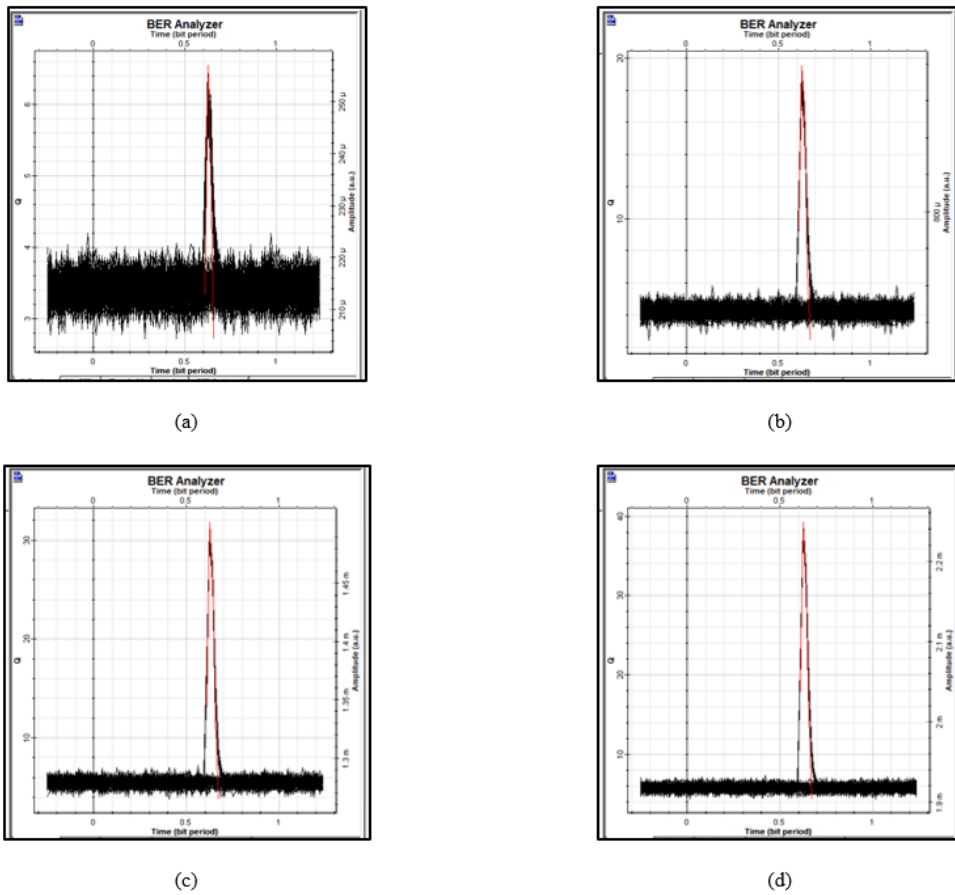


Fig. 8. (a) Eye diagram of the received signal obtained under rainy weather conditions for 10% reflection from the target, measured Q-Factor = 6.56, BER = 2.73e-11. (b) Eye diagram of the received signal obtained under rainy weather conditions for 35% reflection from the target, measured Q-Factor = 19.55, BER = 1.76e-85 (c) Eye diagram of the received signal obtained under rainy weather conditions for 60% reflection from the target, measured Q-Factor = 31.82, BER = 1.27e-222. (d) Eye diagram of the received signal obtained under rainy weather conditions for 90% reflection from the target, measured Q-Factor = 39.26, BER = 1e-253.

Under extremely foggy weather conditions, Figures 9. a, b, c, and d illustrate the eye diagrams of pulses received at a 50 m target distance, with mirror reflection ratios of 10%, 35%, 60%, and 90%, respectively. The obtained eye diagrams clearly demonstrate that increasing the reflection ratio improves optical received signal quality in extremely foggy weather conditions, highlighting the critical role of this parameter in the performance of LiDAR-FSO systems.

Although the Q-Factor achieved at each reflection ratio is sufficient for reliable detection of the LiDAR back-reflected pulse, it has been observed that the noise intensity in extremely foggy weather is significantly higher for all reflection ratios compared to clear and rainy weather conditions. Specifically, at a 10% reflection rate, the noise level increases further, making the signal detection process considerably more challenging than in clear or rainy weather.

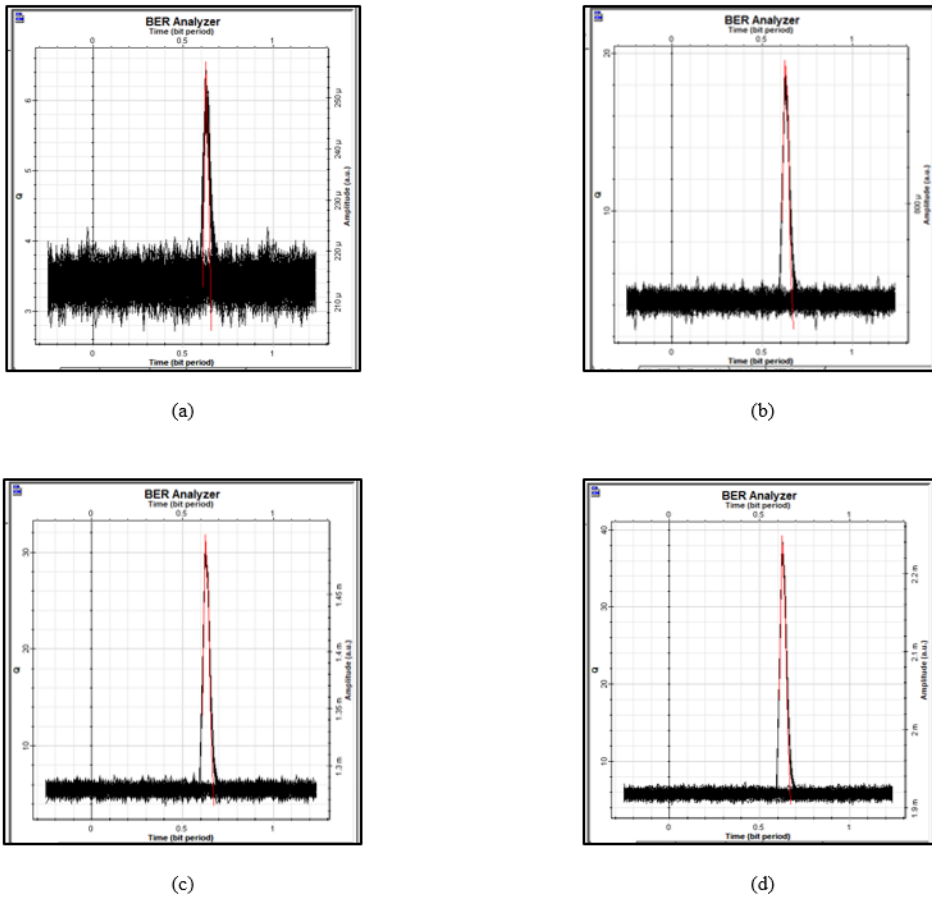


Fig. 9. (a) Eye diagram of the received signal obtained under foggy weather conditions for 10% reflection from the target, measured Q-Factor = 5.82, BER = 2.85e-9. (b) Eye diagram of the received signal obtained under foggy weather conditions for 35% reflection from the target, measured Q-Factor = 19.45, BER = 1.55e-84. (c) Eye diagram of the received signal obtained under foggy weather conditions for 60% reflection from the target, measured Q-Factor = 25.89, BER = 4.01e-148. (d) Eye diagram of the received signal obtained under foggy weather conditions for 90% reflection from the target, measured Q-Factor = 36.6, BER = 1e-253.

3. Potential applications and discussion

Although FSO systems have recently been widely studied in the context of optical wireless communication, their use in simulating the sensing performance of LIDAR systems has remained limited. In this study, a FSO system model was adapted not for analyzing the data transmission performance, but for evaluating the effects of atmospheric losses and target surface reflection characteristics on the performance of an optical fiber-based, lensless LiDAR architecture. This distinction highlights a novel analysis method of FSO applied to LiDAR system design and analysis. Based on the findings of this study, a distributed and phased-array fiber-optic LiDAR system is proposed for future implementation, utilizing a 1x4 fiber coupler at the transmitter side with optimized phased output fiber lengths. The transmitter and receiver fiber sides will have coreless fiber tips at the ends as pairs to emit and collect light through a constant aperture diameter of 0.125 mm to provide short-range sensing enhancement in autonomous vehicles. In this

design, the lensed structure used in conventional LiDAR systems will be eliminated and coreless fiber tips with constant aperture sizes will be used for emitting and collecting light. In this way, the need for precise optical alignment at the transmitter/receiver pairs will be alleviated and the compactness of the system will be enhanced, facilitating its integration into autonomous vehicles.

In literature, there are some studies exhibiting similar performance analyses for LiDAR systems comparable with the results presented here. Table 2 presents a general performance comparison of the proposed system with some existing systems although the proposed system has a fully fiber optical based and lensless structure with 0.125 mm coreless fiber tips as the transmitter and receiver. The proposed system has a moderate lidar range performance at 1550 nm signal wavelength, although it has the smallest aperture size and a very compact structure without a need to a lensed output design. The laser type for the proposed system can be fiber laser or fiber pigtailed diode laser operating at the most popular wavelengths of 905 nm, 940 nm, 980 nm or 1550 nm.

The simulations realized in the study have certain assumptions which can be seen as a shortcoming in performing precise modeling. Firstly, the FSO/LiDAR system model was constructed using the characteristics of high peak power pulsed laser sources. Although an erbium doped fiber amplifier (EDFA) was also used in the system to further increase the output power at 1550 nm and resemble to the practical pulsed diode laser powers, such amplifiers are not always necessary in practical applications due to the availability of commercial diode lasers operating at 900-1000 nm. Therefore, the dominant noise component of the system is usually laser source induced Relative Intensity Noise (RIN). In a different study presenting the experimental performance results of the proposed LiDAR system, dynamic variations, atmospheric turbulence fluctuations, multipath interference, ambient light noise, and sensor imperfections can be investigated in more detail. Secondly, the main objective of the study is to model the impact of optical signal attenuation on LiDAR system performance under challenging atmospheric conditions such as rain and fog. Advanced noise correction algorithms or signal processing techniques can be included at the receiver side of the system to further enhance the performance of an experimental system.

Table 2. General performance comparison.

Ref.	Wavelength (nm)	Pulse Width (ns)	Aperture size (mm)	Lens Usage	Laser Type	Range (m)
[24]	1550	1	6,5 mm collimator, 1,4 mm receiver.	Coaxial lens.	Fiber laser.	267,2
[25]	650	20	6.35	Aspherical lens.	Diode laser.	100
[26]	1550	69,4	Not specified.	Collimating lens.	Diode laser.	7
[27]	905	50	27	Condenser lens.	Diode laser.	0.35
[28]	1550	0.25	15	Telescope lens.	CW laser.	145
This study	1550	10	0.125	Coreless fiber.	Fiber laser or pigtailed diode laser.	80

4. Conclusion

In this study, the performance of a LiDAR system was analyzed through analogy with Free Space Optical (FSO) communication systems under different atmospheric conditions. The simulations evaluated the effects of reflection ratio (10%, 35%, 60%, and 90%) from the mirror (target) surface and distance between the transmitter/receiver and target on optical received signal performance under clear, rainy, and extremely foggy weather conditions. The pulse transmission performance of the LiDAR system was analyzed based on common FSO communication system

performance figures: Q factor, BER, and eye diagram. At clear weather conditions, the most favorable environment for a LiDAR-FSO transmission system was achieved exhibiting a perfect signal quality with a high Q-Factor and a low BER. Increasing the reflection ratio, particularly at the 90% level, maximized received signal quality. On the other hand, the rainy and extremely weather conditions caused higher signal attenuation and a significant decrease in LiDAR-FSO system performance. However, for the reflection ratios of higher than 35% leads to acceptable received signal qualities with high Q factor and low BER values. Extremely foggy weather conditions exhibited the most negative impact on optical signal quality in LiDAR-FSO system, specifically for low reflection ratios and limit the maximum sensing distance of LiDAR system. These results clearly demonstrate that atmospheric conditions and reflection ratios play a critical role on the LiDAR-FSO system performance. It was also shown for all weather conditions that increasing the sensing distance inversely affect the received pulse quality. In conclusion, the simulation results indicate that analyzing LiDAR system performance through analogy with FSO communication system can provide an effective method for understanding the effects of atmospheric conditions and system parameters. In real LiDAR system applications, rainy and extremely foggy weather conditions may be detrimental on received signal quality and may significantly limit the LiDAR sensing distance. Additional solutions to this problem, such as advanced signal processing techniques, more powerful laser sources or more efficient lens designs can be challenging.

4.1. Future work

This study has involved a LiDAR-FSO simulation structure modeled using coreless fiber tips with 0.125 mm cladding diameter at the ends of the transmission fibers. Experimental validation for the proposed structure has not yet been conducted. However, in the next phase, a distributed phased-arrayed fiber-optic LiDAR system will be experimentally designed using a 1x4 fiber coupler with phased output lengths and coreless fiber tip designs as transmitter and receiver apertures. Beside the experimental studies, dynamic variations, atmospheric turbulence fluctuations, multipath interference, ambient light noise, and sensor imperfections will be theoretically investigated in detail. The goal is to validate the simulation outputs under real atmospheric and environmental conditions. This validation study will aim to enhance the practical applicability of the proposed system and improve the reliability of the simulation results.

Acknowledgements

This research did not receive any specific grant from funding agencies in the public, commercial, or non-profit organizations.

Author Contribution

B.K., Conceptualization, methodology, simulation, data analysis, writing – original draft. A.A., Supervision, validation, writing – review & editing, project administration. Both authors read and approved the final version of the manuscript.

References

- [1] F. Scotti et. al., "Dual use architecture for innovative lidar and free space optical communications," *Applied Optics*, vol. 56, no. 31, pp. 8811-8815, 2017, doi:10.1364/AO.56.008811.
- [2] Bouchet, Olivier, et al. *Free-space optics: propagation and communication*. Vol. 91. John Wiley & Sons, 2010.
- [3] S. Bloom, E. Korevaar, J. Schuster, and H. Willebrand, "Understanding the performance of free-space optics," *Journal of Optical Networking*, vol. 2, no. 6, pp. 178-200, June 2003.
- [4] Wahab, Fauzi Abdul, et al. "Multiple transmitters & receivers for free space optical communication link performance analysis." *Journal of Telecommunication, Electronic and Computer Engineering (JTEC)*, vol.8, no.5, pp. 29-32, 2016, <https://jtec.utem.edu.my/jtec/article/view/731>.
- [5] Ghassemlooy, Zabih, Wasu Popoola, and Sujun Rajbhandari. *Optical wireless communications: system and channel modelling with Matlab®*.

CRC press, 2019.

- [6] X. Zhu and J. M. Kahn, "Free-space optical communication through atmospheric turbulence channels," *IEEE Transactions on Communications*, vol. 50, no. 8, pp. 1293-1300, 2002.
- [7] Wu, X., Liu, P. and Matsumoto, M., "A study on atmospheric turbulence effects in full-optical free space communication systems", In *14th International Conference on Wireless Communications Networking and Mobile Computing (WiCOM)*, IEEE, 2010, pp. 1-5.
- [8] X. Yang, W. Chunyang and L. Xuelian. "Research on the Attenuation Characteristics of LiDAR Transmission Energy in Different Atmospheric Environments." *Atmosphere*, vol.16, no.2/210, 2025, doi:10.3390/atmos16020210
- [9] Al-Dabbagh, Rasha, and Hamed Al-Raweshidy. "Millimeter-wave transmission technologies over fiber/fso for 5g+ networks." *2021 IEEE 11th International Conference on Consumer Electronics (ICCE-Berlin)*. IEEE, 2021.
- [10] Elfikky, Abdelrahman, et al. "Spatial diversity-based FSO links under adverse weather conditions: performance analysis." *Optical and Quantum Electronics*, vol.56, no.826, pp2-19, 2024, doi:10.1007/s11082-024-06625-y.
- [11] Zhang, Yu-Ge, et al. "Study on laser scattering depolarization characteristics of typical aerosol particles." *Optics Communications*, 518:128183, 2022.
- [12] L. You, and J. I. Guzman. "Lidar for autonomous driving: The principles, challenges, and trends for automotive lidar and perception systems." *IEEE Signal Processing Magazine*, vol.37, no.4, pp. 50-61, 2020, doi: 10.1109/MSP.2020.2973615.
- [13] Y. Li, P. Duthon, M. Colomb and J. Ibanez-Guzman, "What Happens for a ToF LiDAR in Fog?," in *IEEE Transactions on Intelligent Transportation Systems*, vol. 22, no. 11, pp. 6670-6681, Nov. 2021.
- [14] M. Kuttila, P. Pyykönen, W. Ritter, O. Sawade and B. Schäufele, "Automotive LIDAR sensor development scenarios for harsh weather conditions," *2016 IEEE 19th International Conference on Intelligent Transportation Systems (ITSC)*, Rio de Janeiro, Brazil, 2016, pp. 265-270.
- [15] B. Kaya, A. Altuncu. "Analysis Of The Effect Of Transmitter And Receiver Lens Aperture On System Performance In An Fso Communication System" *14th International Congress On Engineering, Architecture And Design*. 28-29 December 2024.
- [16] Lambert, Jacob, et al. "Performance analysis of 10 models of 3D LiDARs for automated driving." *IEEE Access*, vol.8, no.2169-3536, pp. 131699-131722. 2020, doi: 10.1109/ACCESS.2020.3009680.
- [17] T. Zeng, J. Ji, L. Sun and Y. Song, "OCDMA-Based LiDAR Systems: Reducing False Alarm Probabilities in Autonomous Driving," in *IEEE Photonics Journal*, 2024. doi: 10.1109/JPHOT.2024.3524410.
- [18] Moradi, Hassan, et al. "BER analysis of optical wireless signals through lognormal fading channels with perfect CSI." *2010 17th International Conference on Telecommunications*. IEEE, 2010.
- [19] Otgonbayar, Zambaga, et al. "Designing LiDAR-Detectable Dark-Tone Materials with High Near-Infrared Reflectivity for Autonomous Driving: A Comprehensive Review." *Advanced Functional Materials*, vol.35 no. 2414876, pp.2-28, 2025, , doi:10.1002/adfm.202414876.
- [20] Killinger, Dennis. "Free space optics for laser communication through the air." *Optics and photonics news*, vol.13, no.10, pp.36-42, 2002, doi:10.1364/OPN.13.10.000036.
- [21] K. Hemani, V. K. Jain, and S. Kar. *Free space optical communication*. Vol. 60. ISSN, 1935-3847, New Delhi: Springer India, 2017.
- [22] Farid, A.A., Hranilovic, S, "Outage Capacity Optimization for Free-Space Optical Links With Pointing Errors", *Journal of Lightwave Technology*, vol. 25, no. 7, pp. 1702-1710, July 2007
- [23] Andrews, Larry C., and Ronald L. Phillips. "Laser beam propagation through random media." *Laser Beam Propagation Through Random Media: Second Edition*, 2005.
- [24] Kim, Duck-Lae, Hyun-Woo Park, and Yoon-Mo Yeon. "Analysis of optimal detection range performance of LiDAR systems applying coaxial optics." *Heliyon*, vol.8, no.12, 2022, doi:10.1016/j.heliyon.2022.e12493.
- [25] Nguyen, Thanh-Tuan, et al. "Improvement of accuracy and precision of the lidar system working in high background light conditions." *Electronics*, 11.1, 2021: 45.
- [26] Mingshi, Zhang, et al. "Phase-modulated continuous-wave coherent ranging method for optical phased array lidar." *Optics Express*, vol.31, no.4, pp.6514-6528, 2023, doi:10.1364/OE.477952.
- [27] Wang, Dingkang, et al. "A miniature LiDAR with a detached MEMS scanner for micro-robotics." *IEEE Sensors Journal*, vol.21, no.19, pp.21941-21946, 2021, doi: 10.1109/JSEN.2021.3079426.
- [28] Sharma, Abhishek, et al. "Measurement of target range and Doppler shift by incorporating PDM-enabled FMCW-based photonic radar." *Optik*, vol.262, no. 169191, 2022, doi:10.1016/j.ijleo.2022.169191.